Inorganic Chemistry
Article

Inorg. Chem. **2010**, *49*, 9809–9822 **9809**
DOI: 10.1021/ic101124q

Hydride Ion Transfer from Ruthenium(II) Complexes in Water: Kinetics and Mechanism

Carol Creutz,*,† Mei H. Chou,† Hua Hou,‡ and James T. Muckerman†

†*Chemistry Department, Brookhaven National Laboratory, Upton, New York 11973-5000, United States, and*
‡*College of Chemistry and Molecular Sciences, Wuhan University, Wuhan, 430072, P. R. China*

Received June 3, 2010

Reactions of hydride complexes of ruthenium(II) with hydride acceptors have been examined for Ru(terpy)(bpy)H^+, Ru(terpy)(dmb)H^+, and Ru(η^6-C_6Me_6)(bpy)$(H)^+$ in aqueous media at 25 °C (terpy = 2,2′;6′,2″-terpyridine, bpy = 2,2′-bipyridine, dmb = 4,4′-dimethyl-2,2′-bipyridine). The acceptors include CO_2, CO, CH_2O, and H_3O^+. CO reacts with Ru(terpy)(dmb)H^+ with a rate constant of 1.2 (0.2) $\times$ 10^1 M^{-1} s^{-1}, but for Ru(η^6-C_6Me_6)(bpy)$(H)^+$, the reaction was very slow, $k \leq 0.1$ M^{-1} s^{-1}. Ru(terpy)(bpy)H^+ and Ru(η^6-C_6Me_6)(bpy)$(H)^+$ react with CH_2O with rate constants of $(6 \pm 4) \times 10^6$ and 1.1 $\times$ 10^3 M^{-1} s^{-1}, respectively. The reaction of Ru(η^6-C_6Me_6)(bpy)$(H)^+$ with acid exhibits straightforward, second-order kinetics, with the rate proportional to [Ru(η^6-C_6Me_6)(bpy)$(H)^+$] and [H_3O^+] and k = 2.2 $\times$ 10^1 M^{-1} s^{-1} (μ = 0.1 M, Na_2SO_4 medium). However, for the case of Ru(terpy)(bpy)H^+, the protonation step is very rapid, and only the formation of the product Ru(terpy)(bpy)$(H_2O)^{2+}$ (presumably via a dihydrogen or dihydride complex) is observed with a k_{obs} of ca. 4 s^{-1}. The hydricities of HCO_2^-, HCO^-, and H_3CO^- in water are estimated as +1.48, −0.76, and +1.57 eV/molecule (+34, −17.5, +36 kcal/mol), respectively. Theoretical studies of the reactions with CO_2 reveal a "product-like" transition state with short C−H and long M−H distances. (Reactant) Ru−H stretched 0.68 Å; (product) C−H stretched only 0.04 Å. The role of water solvent was explored by including one, two, or three water molecules in the calculation.

Introduction

Mediators are needed in the solar generation of fuels to couple photogenerated electrons to proton-coupled, electron-transfer reactions that lower the barriers for generation of H_2, through reduction of the protons in water and/or carbon dioxide to methanol.[1] Metal hydride complexes can potentially fulfill this role.[2,3] The homogeneous reduction of CO_2 by highly reducing metal centers[4] via M−CO_2 adducts and by insertion into metal hydride bonds to yield the complexed formate[5−7] ion has been studied since the early 1980s.[8] Further homogeneous reduction of free CO[9] (with $NaBH_3CN$)[10,11] to CH_2O and of CH_2O to CH_3OH has received less attention.[12] Hydride complexes of d^6 metal centers (Mo(0),[13] Re(I),[7,14] Ru(II),[15] Rh(III), Ir(III), Fe(II)[16−18]) reduce ketones to alcohols and CO_2 to formate in organic solvents. Such metal hydride complexes have also been invoked as intermediates in the electroreduction of CO_2 with, for example, $Ru(bpy)_2(CO)$ as a catalyst precursor.[19] Homogeneous catalysis of CO_2 reduction in water[20−23] presumably

*To whom correspondence should be addressed. E-mail: ccreutz@bnl.gov.

(1) *Basic Research Needs for Solar Energy Utilization, Report of the Basic Energy Sciences Workshop on Solar Energy Utilization*, April 18−21, 2005; Office of Science, U.S. DOE: Bethesda, MD, 2005.
(2) Sutin, N.; Creutz, C.; Fujita, E. *Comments Inorg. Chem.* **1997**, *19*, 67–92.
(3) Fukuzumi, S. *Eur. J. Inorg. Chem.* **2008**, 1351–1362.
(4) Fisher, B.; Eisenberg, R. *J. Am. Chem. Soc.* **1980**, *102*, 7363–7366.
(5) Sullivan, B. P.; Bolinger, C. M.; Conrad, D.; Vining, W. J.; Meyer, T. J. *J. Chem. Soc., Chem. Commun.* **1985**, 1414–1416.
(6) Sullivan, B. P.; Meyer, T. J. *Chem. Commun.* **1984**, 1244–5.
(7) Sullivan, B. P.; Meyer, T. J. *Organometallics* **1986**, *5*, 1500–1502.
(8) Benson, E. E.; Kubiak, C. P.; Sathrum, A. J.; Smieja, J. M. *Chem. Soc. Rev.* **2009**, *38*, 89–99.
(9) Klingler, R. J.; Rathke, J. W. *Prog. Inorg. Chem.* **1991**, *39*, 113–180.
(10) Bodnar, T.; Coman, E.; Menard, K.; Cutler, A. *Inorg. Chem.* **1982**, *21*, 1275–1277.
(11) Lin, Y. C.; Milstein, D.; Wreford, S. S. *Organometallics* **1983**, *2*, 1461–3.
(12) Gambarotta, S.; Strologo, S.; Floriani, C.; Chiesi-Villa, A.; Guastini, C. *J. Am. Chem. Soc.* **1985**, *107*, 6278–6282.
(13) Liang, F.; Schmalle, H. W.; Fox, T.; Berke, H. *Organometallics* **2003**, *22*, 3382–3393.
(14) Nietlispach, D.; Veghini, D.; Berke, H. *Helv. Chim. Acta* **1994**, *77*, 2197–2208.
(15) Clapham, S. E.; Hadzovic, A.; Morris, R. H. *Coord. Chem. Rev.* **2004**, *248*, 2201–2237.
(16) Field, L. D.; Lawrenz, E. T.; Shaw, W. J.; Turner, P. *Inorg. Chem.* **2000**, *39*, 5632–5638.
(17) Mikhailine, A.; Lough, A. J.; Morris, R. H. *J. Am. Chem. Soc.* **2009**, *131*, 1394–1395.
(18) Casey, C. P.; Guan, H. *J. Am. Chem. Soc.* **2007**, *129*, 5816–5817.
(19) Pugh, J. R.; Bruce, M. R. M.; Sullivan, B. P.; Meyer, T. J. *Inorg. Chem.* **1991**, *30*, 86–91.
(20) Himeda, Y. *Eur. J. Inorg. Chem.* **2007**, 3927–3941.
(21) Himeda, Y.; Onozawa-Komatsuzaki, N.; Sugihara, H.; Arakawa, H.; Kasuga, K. *Organometallics* **2004**, *23*, 1480–1483.

Published on Web 10/08/2010

involves such hydride complexes. Despite the desirability of water solvent and its utilization in catalytic reductions,[24−26] studies of metal hydride complexes in water have been rather limited: they include Rh porphyrin[27] and macrocycle[28] complexes, $(Cp)_2Mo(H)(OH_2)^+$,[29] $(C_5H_4(CO_2^-)(CO)_2LW$ (L = CO, PMe_3),[30] $Fe(P_2)_2X_2$-type complexes (P_2 = a chelating, water-solubilizing phosphine),[31] Ru(η^6-C_6Me_6)(bpy)$(H)^+$,[32] $CpRu(TPA)_2H$ (TPA = 1,3,5-triaza-7-phosphaazamantane),[33] (η^6-C_6Me_6)(bpy)RhH^+,[34,35] and (η^6-C_6Me_6)Ir(bpy)H^+.[32,36]

We are interested in the chemistry of hydride complexes of d^6 metal centers in water.[37,38] For the most part, the aqua complexes of the water-soluble derivatives above have been shown to react directly with hydrogen and/or the formate ion to yield the corresponding metal hydride complex. Then, the hydride complex can be used to transfer the hydride ion (often enantiospecifically) to ketones and other unsaturated organic molecules. The thermodynamics of reduction of ketones and carbon dioxide do not differ greatly (see Table S0, Supporting Information): apart from the hydrogenation of formaldehyde to methanol, the overall hydrogenation of CO_2 and its reduction products is more thermodynamically demanding (by as much as 7.6 kcal/mol) than the hydrogenation of ketones, exemplified by acetone. This suggested to us the use of d^6 metal hydrides, competent in transfer hydrogenation, as mediators for the reduction of carbon dioxide to formate or methanol and of H^+ to H_2. Furthermore, the reverse of CO_2 reduction to formate, decarboxylation of formic acid, is of interest as a source of hydrogen from formic acid, a viable hydrogen storage medium.[39]

Chart 1

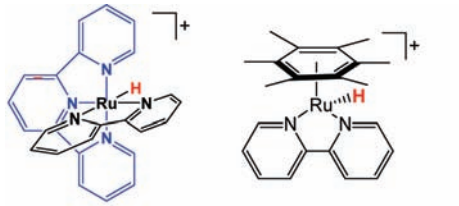

The reaction of CO_2 with Ru(II) hydrides, an apparent insertion reaction, has received some theoretical attention.[26,40−44] An accelerating role for water has been ascribed to hydrogen bonding stabilization of increasing negative charge on oxygen in CO_2 as the hydride ion is transferred to the carbon.[43] In another study, water was found to serve as both a ligand and a proton source.[45]

In the present report, we describe kinetics and mechanistic studies of hydride transfer reactions of a few hydride complexes, principally, Ru(terpy)(bpy)H^+ and Ru(η^6-C_6Me_6)(bpy)$(H)^+$ (terpy = 2,2′;6′,2″-terpyridine, bpy = 2,2′-bipyridine), which are depicted in Chart 1. Preliminary accounts of their reactions with CO_2 have been reported.[37,38] Here, we report our results of studies with hydride acceptors H_3O^+, CO_2, CO, and CH_2O in water. Theoretical studies of the reactions with CO_2 have been conducted in an effort to clarify the mechanisms.

Experimental Section

Materials. The hydride complexes [Ru(terpy)(bpy)H][PF_6] and [Ru(terpy)(dmb)H][PF_6] (dmb = 4,4′-dimethyl-2,2′bipyridine) were prepared from [Ru(terpy)(bpy)Cl][PF_6][46] and [Ru(terpy)(dmb)Cl][PF_6], respectively, as described in the literature.[47] [Ru(terpy)(bpy)H][PF_6] ^{1}H NMR (DMS-d_6): δ −14.7. IR (KBr pellet): ν_H 1827 cm^{-1}, ν_D 1292 cm^{-1}. UV−vis (H_2O): 500 nm (8.5×10^3 M^{-1} cm^{-1}). Mass spec: m/z 490 ^{102}Ru. The solubility of the PF_6^- salt is not large in water, ca. 0.33 mM. It was noted that higher quantities could apparently be "dissolved" by ultrasonication, but these suspensions gave rise to confusing absorbance changes as the suspension dissolved and reacted. The triflate salt of this hydride exhibits a strikingly broadened M−H stretch (KBr pellet, see Supporting Information) and, on the basis of its ^{1}H NMR, appears to be a hydride-bridged dimer analogous to that found for $(CO)_3$(bpy)Re^I.[48,49]

[Ru(terpy)(dmb)H][PF_6]. ^{1}H NMR (DMSO d_6): δ −14.9 (see Supporting Information for full spectrum). IR (KBr pellet): ν_H 1857 cm^{-1}. UV−vis in water: 480 nm (6.9×10^3 M^{-1} cm^{-1}), 315 (2.4×10^4 M^{-1} cm^{-1}), 286 (2.6×10^4 M^{-1} cm^{-1}). Mass spec: m/z 668 ^{102}Ru, [Ru(terpy)(dmb)H][CF_3SO_3] in CH_3CN. The PF_6 salt is barely soluble in water (18.7 μM). UV−vis, infrared, ^{1}H NMR, and mass spectra of [Ru(terpy)(dmb)H][PF_6] are presented in the Supporting Information.

Ru(η^6-C_6Me_6)(bpy)(H)[CF_3SO_3]. (η^6-C_6Me_6)$_2Ru_2Cl_4$ was prepared from the p-cymene dimer (Aldrich) using the literature procedure.[50] (η^6-C_6Me_6)$Ru(H_2O)^{2+}$ was prepared by treating

(22) Himeda, Y.; Onozawa-Komatsuzaki, N.; Sugihara, H.; Kasuga, K. *J. Photochem. Photobiol. A, Chem.* **2006**, *182*, 306–309.
(23) Himeda, Y.; Onozawa-Komatsuzaki, N.; Sugihara, H.; Kasuga, K. *Organometallics* **2007**, *26*, 702–712.
(24) Laurenczy, G.; Joó, F.; Nadasdi, L. *Inorg. Chem.* **2000**, *39*, 5083–5088.
(25) Horvath, H.; Laurenczy, G.; Katho, A. *J. Organomet. Chem.* **2004**, *689*, 1036–1045.
(26) Urakawa, A.; Jutz, F.; Laurenczy, G.; Baiker, A. *Chem.—Eur. J.* **2007**, *13*, 3886–3899.
(27) Fu, X. F.; Li, S.; Wayland, B. B. *Inorg. Chem.* **2006**, *45*, 9884–9889.
(28) Bakac, A. *Dalton Trans.* **2006**, 1589–1596.
(29) Breno, K. L.; Ahmed, T. J.; Pluth, M. D.; Balzarek, C.; Tyler, D. R. *Coord. Chem. Rev.* **2006**, *250*, 1141–1151.
(30) Cabelli, D. E.; Shafiq, F.; Creutz, C.; Bullock, R. M. *Organometallics* **2001**, *20*, 3729–3737.
(31) Gilbertson, J. D.; Szymczak, N. K.; Crossland, J. L.; Miller, W. K.; Lyon, D. K.; Foxman, B. M.; Davis, J.; Tyler, D. R. *Inorg. Chem.* **2007**, *46*, 1205–1214.
(32) Ogo, S.; Kabe, R.; Hayashi, H.; Harada, R.; Fukuzumi, S. *Dalton Trans.* **2006**, 4657–4663.
(33) Mebi, C. A.; Nair, R. P.; Frost, B. J. *Organometallics* **2007**, *26*, 429–438.
(34) Koelle, U. *New J. Chem.* **1992**, *16*, 157–169.
(35) Steckhan, E.; Herrmann, S.; Ruppert, R.; Dietz, E.; Frede, M.; Spika, E. *Organometallics* **1991**, *10*, 1568–1577.
(36) Steckhan, E.; Herrmann, S.; Ruppert, R.; Dietz, E.; Frede, M.; Spika, E. *Organometallics* **1991**, *10*, 1568–1577.
(37) Creutz, C.; Chou, M. H. *J. Am. Chem. Soc.* **2007**, *129*, 10108–10109.
(38) Creutz, C.; Chou, M. H. *J. Am. Chem. Soc.* **2009**, *131*, 2794–2795.
(39) Boddien, A.; Loges, B. r.; Galîrtner, F.; Torborg, C.; Fumino, K.; Junge, H.; Ludwig, R.; Beller, M. *J. Am. Chem. Soc.* **2010**, *132*, 8924–8934.
(40) Musashi, Y.; Sakaki, S. *J. Am. Chem. Soc.* **2000**, *122*, 3867–3877.
(41) Ohnishi, Y.; Matsunaga, T.; Nakao, Y.; Sato, H.; Sakaki, S. *J. Am. Chem. Soc.* **2005**, *127*, 4021–4032.
(42) Ohnishi, Y. Y.; Nakao, Y.; Sato, H.; Sakaki, S. *Organometallics* **2006**, *25*, 3352–3363.
(43) Yin, C. Q.; Xu, Z. T.; Yang, S. Y.; Ng, S. M.; Wong, K. Y.; Lin, Z. Y.; Lau, C. P. *Organometallics* **2001**, *20*, 1216–1222.
(44) Urakawa, A.; Iannuzzi, M.; Hutter, J.; Baiker, A. *Chem.—Eur. J.* **2007**, *13*, 6828–6840.
(45) Kovacs, G.; Schubert, G.; Joo, F.; Papai, I. *Catal. Today* **2006**, *115*, 53–60.
(46) Takeuchi, K. J.; Thompson, M. S.; Pipes, D. W.; Meyer, T. J. *Inorg. Chem.* **1984**, *23*, 1845–1851.
(47) Konno, H.; Kobayashi, A.; Sakamoto, K.; Fagalde, F.; Katz, N. E.; Saitoh, H.; Ishitani, O. *Inorg. Chim. Acta* **2000**, *299*, 155–163.
(48) Hawecker, J.; Lehn, J. M.; Ziessel, R. *Helv. Chim. Acta* **1986**, *69*, 1990–2012.
(49) Guilhem, J.; Pascard, C.; Lehn, J. M.; Ziessel, R. *J. Chem. Soc., Dalton Trans.* **1989**, 1449–1454.

(η^6-C_6Me_6)$_2Ru_2Cl_4$ (150 mg, 0.225 mmol) with Ag_2SO_4 (141 mg, 0.45 mmol) in 30 mL of water, stirring with intermittent ultrasonication over 1 h, during which the orange solid dissolved.[50] The solution of the aqua complex was filtered from the AgCl, and 70.5 mg of bpy was added. The resulting solution was stirred at room temperature overnight, and the water was evaporated to give the solid sulfate salt, Ru(η^6-C_6Me_6)(bpy)(H_2O)[SO_4].[32] To prepare the hydride complex, 96 mg of Ru(η^6-C_6Me_6)(bpy)(H_2O)[SO_4] in 15 mL of pH 7 water under argon was treated with $NaBH_4$ (8 mg in 1 mL of water). The solution was filtered from a black solid, and 2 mL of 1 M lithium triflate was added to give Ru(η^6-C_6Me_6)(bpy)(H)[CF_3SO_3] as an orange solid.[51] The properties found were in good agreement with those published earlier: ^{1}H NMR: δ −6.98 (DMSO d_6) (−7.45 (H_2O)[51]). IR (KBr pellet): ν_H 1908 cm^{-1}.[52] UV−vis in water: 480 nm (6.9×10^3 M^{-1} cm^{-1}), 315 (2.4×10^4 M^{-1} cm^{-1}), 286 (2.6×10^4 M^{-1} cm^{-1}).

$Na_2Re(dcb)(CO)_3H$ was prepared from $Re(dcbH_2)(CO)_3Cl$[53] and sodium borohydride[6] following literature methods. ESI-MS in 50:50 MeOH/H_2O: m/z 1117 [($Na_2Re(dcb)(CO)_3H)_2$ − 3H] (see Supporting Information).

Methods. The hydride complexes are not noticeably oxygen sensitive but must be rigorously protected from the carbon dioxide in air. Thus, reagents were prepared under argon with freshly drawn millQ water and transferred with use of syringe techniques. Kinetics runs were carried out with 0.03 to 0.1 mM RuH^+ and the hydride acceptors in at least 10-fold excess. Experiments with CO used 100% and 50% CO/50% Ar-saturated solutions in water (0.94 and 0.47 mM, respectively). Commerical CO_2/Ar mixtures were used to vary the [CO_2], and the reactions were monitored by diode array on an Applied Photophysics stopped-flow spectrometer for the terpy-containing complexes and conventional mixing on an HP-diode array spectrometer. Mass spectra were monitored on a Thermo Finnigan LCQ MS.

The reactions involving CO_2 were run either at very low ionic strength or at 0.5 M ionic strength. For the low ionic strength experiments, equilibrium data tabulated by Butler (Table 2.1[54]) were used. For 0.5 M ionic strength, we used the following values, interpolated from figures given by Butler:[54] Henry's constant 0.0315, pK_{a1} = 6.01, pK_{a2} = 9.2, and pK_w = 13.7.

Calculations. All calculations were carried out with the Gaussian 03 program package[55] using the MWB28 ECP basis[56−58] for Ru. For carbon dioxide, water molecules, hydride, nitrogen atoms, and the C6 group of Me_6C_6, 6-31G(d,p) basis sets were used; for all of the other carbon and hydrogen atoms, 6-31G basis sets were used. Most calculations employed the hybrid DFT B3LYP method,[59−61] but these were complemented by selected CAS(4,4) calculations.[62−66] Time-dependent B3LYP (TD-B3LYP) calculations were carried out with the Gaussian 03 program in order to predict UV−vis spectra. Gv (298.15 K) was obtained. This is the calculated free energy obtained with the entropic term limited to vibrational contributions. Use of Gv follows the recommendation of Yin et al.,[43] who proposed that only vibrational contributions to the entropy are important in solution where the translational and rotational motions are significantly suppressed.

Scheme 1. Protonation of RuH to produce H_2

$$Ru(terpy)(bpy)H^+ + H_3O^+ \rightleftarrows Ru(terpy)(bpy)H_2^{2+} + H_2O \quad k_f, k_r; K \qquad \text{(i)}$$

$$Ru(terpy)(bpy)H_2^{2+} + H_2O \rightarrow Ru(terpy)(bpy)(H_2O)^{2+} + H_2 \quad k_{H_2} \qquad \text{(ii)}$$

Results

1. Properties of the Complexes. Since a number of studies involve changes of solution pH, we checked the ionization constants of the aqua complexes, a reagent or product in all of the reactions studied, against literature reports for the pK_a's of the aqua complexes, eqs 1 and 2—pK_1 = 10[67] and 9.7[46] (μ = 0.1 M), and pK_2 = 8.6.[32] From 400-nm absorbance data, we determined pK_2 to be 8.0 at 25 °C. We concluded that especially for the experiments at high ionic strengths (in which the aqua ions are expected to be even weaker acids) the hydroxyl complexes should not play a role.

$$Ru(terpy)(bpy)(H_2O)^{2+} \rightleftharpoons Ru(terpy)(bpy)(OH)^+ + H^+ \qquad (1)$$

$$Ru(\eta^6\text{-}C_6Me_6)(bpy)(H_2O)^{2+} \rightleftharpoons Ru(\eta^6\text{-}C_6Me_6)(bpy)(OH)^+ + H^+ \qquad (2)$$

pH-dependent spectra are shown in the Supporting Information.

2. Reactions of Metal Hydride Complexes with Hydride Ion Acceptors. a. Reaction with H^+: MH = Ru(terpy)(bpy)H^+. The reaction of the hydride complex with acid yields H_2 (≥60% yield[37]) and Ru(terpy)(bpy)(H_2O)$^{2+}$, verified by UV−vis and ESI MS.[37] The rates of reaction of Ru(terpy)(bpy)H^+ with H^+ were examined in a 0.05 M triflate medium using stopped-flow methods, monitoring the UV−vis spectrum with a diode array. The results (see Scheme ii) are consistent with a two-step mechanism in which rapid, reversible protonation of the hydride (*i*) is followed by slower loss of dihydrogen to yield the aqua complex (*ii*).

The earliest spectra measured by stopped-flow spectrometry already differed from that of the parent hydride complex, as is shown below for spectra measured at t = 1 ms in Figure 1 (upper left). Thus, stage *i* is too fast to observe. On the basis of this information, we estimate $k_f \geq 10^4$ M^{-1} s^{-1}. From K = 300 M^{-1} (see Figure 3), the value

(50) Bennett, M. A.; Huang, T. N.; Matheson, T. W.; Smith, A. K. *Inorg. Synth.* **1982**, *21*, 74–78.
(51) Hayashi, H.; Ogo, S.; Abura, T.; Fukuzumi, S. *J. Am. Chem. Soc.* **2003**, *125*, 14266–14267.
(52) Zhu, X. Q.; Wang, C. H.; Liang, H.; Cheng, J. P. *J. Org. Chem.* **2007**, *72*, 945–956.
(53) Pfennig, B. W.; Chen, P.; Meyer, T. J. *Inorg. Chem.* **1996**, *35*, 2898–2901.
(54) Butler, J. N. *Carbon Dioxide Equilibria and Their Applications*; Addison-Wesley: Reading, MA, 1982.
(55) Frisch, M. J. et al. *Gaussian 03*, revision B.04; Gaussian, Inc.: Wallingford, CT, 2004. See Supporting Information for full citation.
(56) Hay, P. J.; Wadt, W. R. *J. Chem. Phys.* **1985**, *82*, 270–283.
(57) Wadt, W. R.; Hay, P. J. *J. Chem. Phys.* **1985**, *82*, 284–298.
(58) Hay, P. J.; Wadt, W. R. *J. Chem. Phys.* **1985**, *82*, 299–310.
(59) Becke, A. D. *Phys. Rev. A* **1988**, *38*, 3098–3100.
(60) Lee, C.; Yang, W.; Parr, R. G. *Phys. Rev. B* **1988**, *37*, 785–789.
(61) Miehlich, B.; Savin, A.; Stoll, H.; Preuss, H. *Chem. Phys. Lett.* **1989**, *157*, 200–206.
(62) Hegarty, D.; Robb, M. A. *Mol. Phys.* **1979**, *38*, 1795–1812.
(63) Schlegel, H. B.; Robb, M. A. *Chem. Phys. Lett.* **1982**, *93*, 43–46.
(64) Bernardi, F.; Bottoni, A.; McDouall, J. J. W.; Robb, M. A.; Schlegel, H. B. *Faraday Symp. Chem. Soc.* **1984**, 137–147.
(65) Frisch, M.; Ragazos, I. N.; Robb, M. A.; Schlegel, H. B. *Chem. Phys. Lett.* **1992**, *189*, 524–528.
(66) Yamamoto, N.; Vreven, T.; Robb, M. A.; Frisch, M. J.; Schlegel, H. B. *Chem. Phys. Lett.* **1996**, *250*, 373–378.
(67) Davies, N. R.; Mullins, T. L. *Aust. J. Chem.* **1967**, *20*, 657–668.

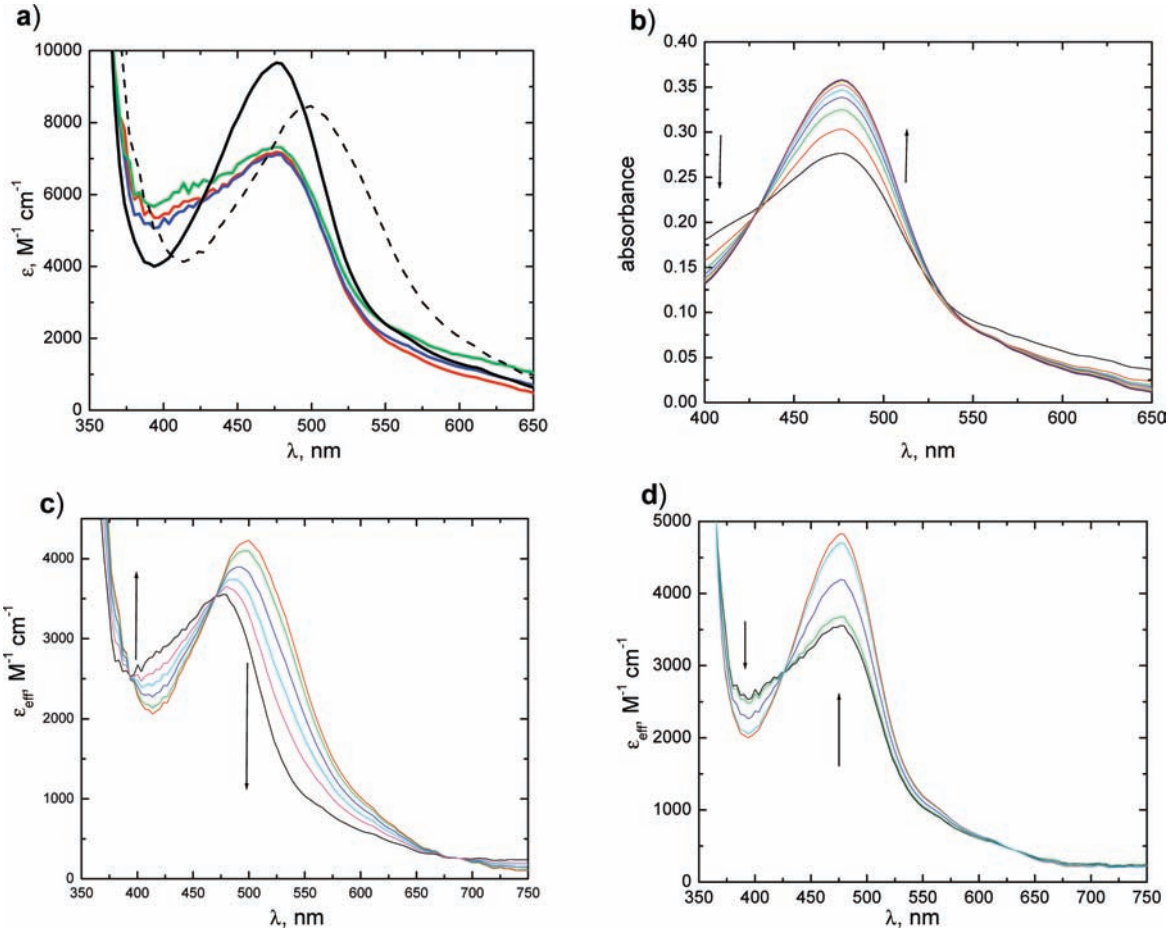

Figure 1. (a) The 1 ms spectra obtained in water (dashed) and 10 (blue), 20 (purple), and 50 (red) mM acid compared with the final spectrum (black) for 50 mM acid; $\mu = 0.05$ M (Li triflate). (b) Spectra obtained every 0.2 s for 1 mM triflic acid. (c) Simulation of spectral changes for the first stage, $RuH^+ + H^+ = RuH_2^{2+}$, obtained by using the initial ε values in water and 0.05 M triflic acid to calculate (simulate) the spectra of mixtures of various compositions: black, 100% RuH_2^{2+}; red, 100% RuH^+; green, 90% RuH^+/10% RuH_2^{2+}; purple, 70% RuH^+/30% RuH_2^{2+}; turquoise, 50% RuH^+/50% RuH_2^{2+}; magenta, 10% RuH^+/90% RuH_2^{2+}. (d) Simulation of spectral changes for the second stage, $RuH_2^{2+} + H_2O = Ru(H_2O)^{2+} + H_2$: black, 100% RuH_2O^{2+}; red, 100% RuH_2^+; green, 90% RuH_2^{2+}/10% RuH_2O^{2+}; purple, 50% RuH_2^{2+}/50% RuH_2O^{2+}; turquoise, 10% RuH_2^{2+}/90% RuH_2O^{2+}.

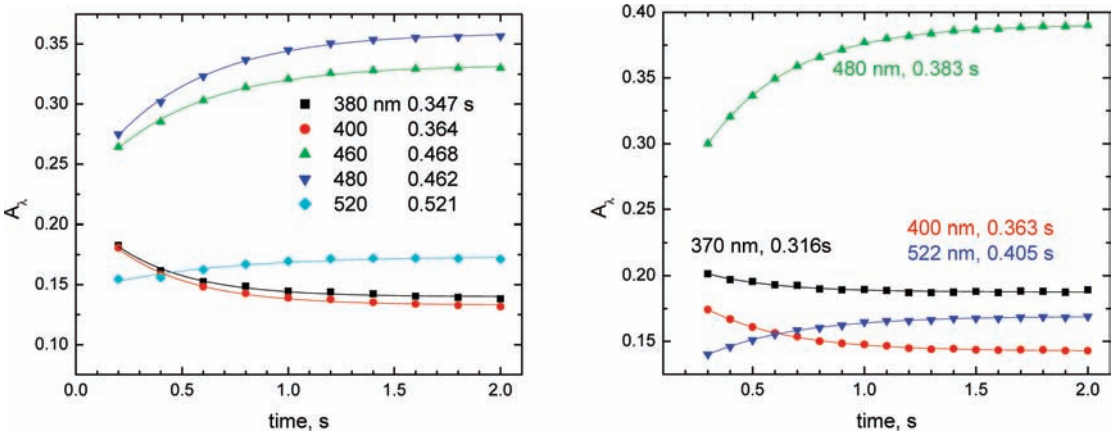

Figure 2. First-order fits to data for stage *ii* at several wavelengths. (Left) 1 mM triflic acid, $\mu = 0.05$ M (Li triflate). The average value of k_{obs} is 2.3 s^{-1}. (Right) 4 mM triflic acid, $\mu = 0.05$ M (Li triflate). The average value of k_{obs} is 2.7 s^{-1}.

$k_r \geq 30$ s^{-1} is obtained. Only the slow second stage in which the aqua complex is formed can be followed spectrophotometrically (Figure 1, upper right). The rate constant for this stage (see Figure 2) is ca. 3 s^{-1} (*vide infra*). Since the absorbance changes for the two stages are confusing because they have opposite signs, we simulated the spectra of mixtures to check this interpretation. To do this, we assumed that pure RuH^+ could be modeled by its absorption spectrum in water, that the initial spectrum of RuH^+ in 0.05 M triflic acid was the spectrum of 100% RuH_2^{2+}, and that the final spectrum in 0.05 M triflic acid was the spectrum of 100% RuH_2O^{2+}. The simulated

spectra, shown in Figure 1c and d, reproduce the spectral changes observed and add support for Scheme ii as a mechanism.

Concerned that triflate might be inducing transient precipitation (see below for the behavior of Ru(η^6-C_6Me_6)(bpy)$(H)^+$), we changed the acid reagent to sulfuric acid at 0.1 M ionic strength (Na_2SO_4). Between 0 and 1 mM, this acid acts as a simple dibasic acid (eq 3). At higher concentrations, the sulfate−bisulfate equilibrium (eq 4) must be taken into account to obtain $[H^+]$.

$$H_2SO_4 + 2H_2O \rightleftharpoons 2H_3O^+ + SO_4^{2-} \qquad (3)$$

$$HSO_4^- + H_2O \rightleftharpoons H_3O^+ + SO_4^{2-} \quad pK_a = 1.92 \qquad (4)$$

Again, we found that, while the final absorption spectra were the same within 10%, striking differences in the early spectra were found, as shown in Figure 4. The variation of the initial spectra with pH implicates a pK_a of ca. 2.8 (see inset) for eq A1.

We tried to observe the protonation *i* at early times, but there was no compelling evidence that this stage was observable, as shown in Figure S10 (Supporting Information). Thus, $k_f \geq 2 \times 10^4$ M^{-1} s^{-1}, and from K = 600 M^{-1} (see Figure 4), $k_r \geq 30$ s^{-1}. Spectral changes with time for pH 5.8 acetate and phosphate buffers are shown in Figure S11 (Supporting Information). The pseudo-first-order rate constants for stage *ii* at different acid concentrations are listed in Table 1 for both triflate and sulfate media. First-order fits to the data for stage *ii* for Ru(terpy)(bpy)H^+ in the sulfate medium are shown in Figure 5.

MH = Ru(η^6-C_6Me_6)(bpy)$(H)^+$. Initial experiments involving mixing of Ru(η^6-C_6Me_6)(bpy)(H)$[CF_3SO_3]$ with triflic acid gave bizarre kinetic traces (see the Supporting Information) that were found to be due to precipitation of the triflate salt of the product aqua complex. As described above, reaction eq 5 was then studied in the sulfate medium:

$$Ru(\eta^6\text{-}C_6Me_6)(bpy)(H)^+ + H_3O^+ \rightarrow Ru(\eta^6\text{-}C_6Me_6)(bpy)(H_2O)^{2+} + H_2 \qquad (5)$$

The spectral changes are illustrated, and the dependence of pseudo-first-order rate constants on acid concentration are presented in Figure 6 and in the Supporting Information. For the plot in Figure 6, the slope and intercept are 43.5 (2) and −0.9(1), so that the rate constant for eq 5 is 2.2 × 10^1 M^{-1} s^{-1}.

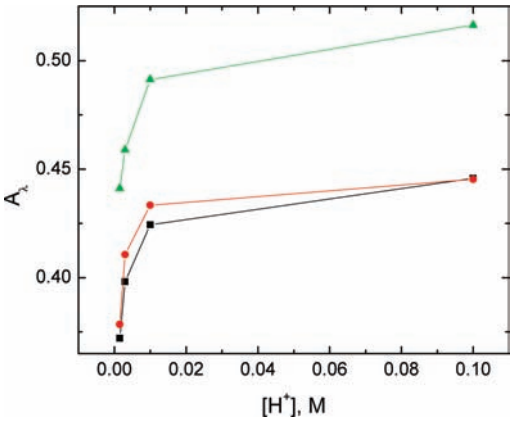

Figure 3. The variation of initial spectra at 476 (green), 500 (red), and 450 nm (black) with pH. This suggests a pK_a of ca. 2.5 in triflate, μ = 0.05 M.

Table 1. Pseudo-First Order Rate Constants for Conversion of Ru(terpy)(bpy)H_2^{2+} to Ru(terpy)(bpy)$(H_2O)^{2+}$ at 25 °C

$[H^+]$, M[a]	k_{obs}, s^{-1}	$[H^+]$, M[b]	k_{obs}, s^{-1}
0.001	2.16	1.99×10^{-6}[c]	0.67
0.002	2.44	1.58×10^{-6}[d]	1.1
0.004	2.61	0.00041	4.3
0.010	3.11	0.00083	4.8
0.020	3.08	0.0022	3.5
0.030	2.92	0.012	4.3
0.040	3.05	0.0167	4.5
0.050	3.18	0.037	3.8

[a] μ = 0.05 M ($LiCF_3SO_3$). [b] μ = 0.10 M (Na_2SO_4/HSO_4^-). [c] Acetate buffer, μ = 0.05 M ($LiCF_3SO_3$), 0.5 mM HAc/5 mM NaAc. [d] μ = 0.05 M ($LiCF_3SO_3$), 5 mM NaH_2PO_4/0.5 mM Na_2HPO_4.

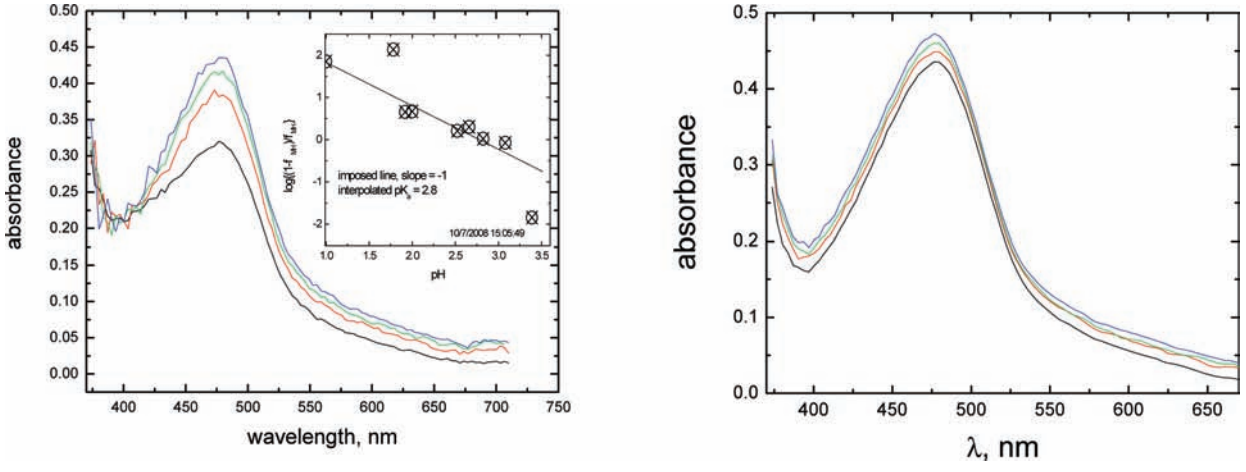

Figure 4. (Left) Initial spectra determined in 0.5 (black), 1.0 (red), 2.5 (green), and 10 (blue) mM sulfuric acid. Inset: 476-nm data, apparent pK_a of 2.8. The absorbance values in the main figure were used to calculate the ratio of $[RuH^+]$ to $[RuH_2^{2+}]$, $(1 - f_{MH})/f_{MH}$, with the assumption that the sum of the concentrations is constant on the time scale of the measurement. (Right) Final spectra corresponding to the initial spectra at the left. The total absorbance change measured decreased with increasing acid concentration.

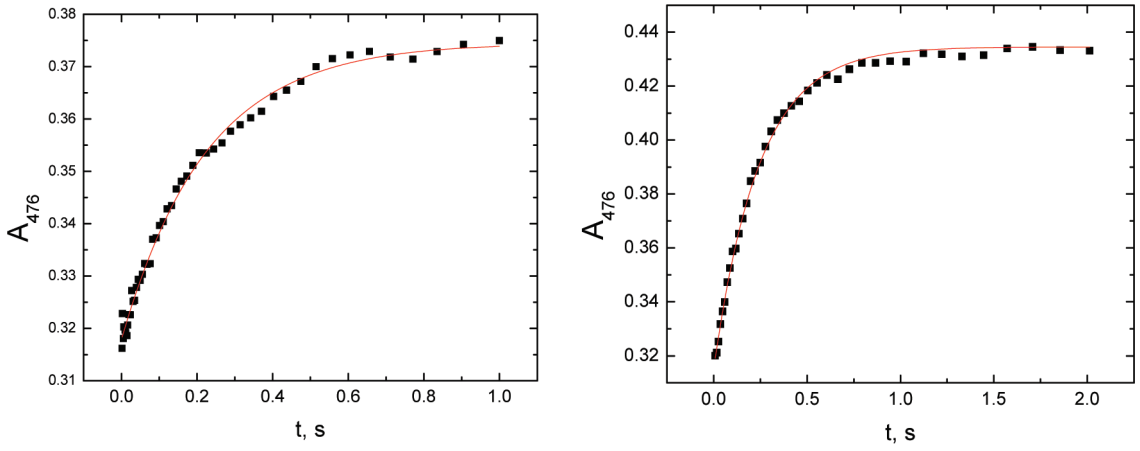

Figure 5. First-order fits to data for stage *ii* for Ru(terpy)(bpy)H^+ in the sulfate medium. Absorbance at 476 nm vs time for (left) 0.02 M H_2SO_4 (k_{obs} = 4.5 s^{-1}) and (right) 0.5 mMH_2SO_4 and 0.03 M Na_2SO_4 (k_{obs} = 4.1 s^{-1}).

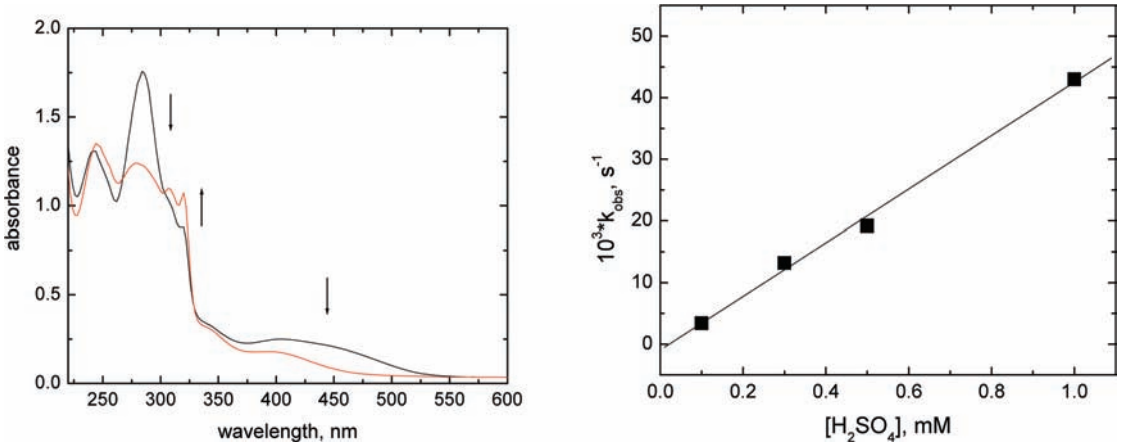

Figure 6. Net spectral change for the reaction [Ru(η^6-C^6Me^6)(bpy)(H)]TFMS in 0.03 M Na_2SO_4 with 0.3 mM sulfuric acid (left) and the dependence of the pseudo-first-order rate constants for the reaction on acid concentration (right).

b. Reaction with CO_2. The kinetics of the reaction of CO_2 with Ru(terpy)(bpy)H^+ and Ru(η^6-C_6Me_6)(bpy)-$(H)^+$ were reported earlier.[37,38] This reaction yields a formate complex, which subsequently undergoes aquation (eq 6).

$$RuH^+ + CO_2 \underset{k_{-1}}{\overset{k_1}{\rightleftharpoons}} RuOCH(O)^+ \underset{k_{-2}}{\overset{k_2}{\rightleftharpoons}} Ru(H_2O)^{2+} + HCO_2^- \quad (6)$$

Ogo et al. earlier reported[51] that the reaction rate observed for eq 6 accelerates with [H^+] when the solution acidity increases from 0.1 to 0.6 mM. We note that at least part of this acceleration is due to the reaction of the hydride complex with H^+ itself, eq 5. This is supported by the observation (Table S2, Supporting Information) that the yield of H_2 doubles from 0.09 at pH 4.8 to 0.18 at pH 3.8 (conditions as described by Ogo et al., but with 10 times greater [Ru(η^6-C_6Me_6)(bpy)$(H)^+$] to facilitate H_2 determination).

The isotope effect k_H/k_D on the rate constant for formate binding to Ru(η^6-C_6Me_6)(bpy)$(H_2O)^{2+}$, k_{-2} (eq 6), is 1.0 within our errors; however, k_{-1}, which is obtained from the limiting rate at a high formate concentration, exhibits a small, normal isotope effect k_H/k_D = 1.15(0.1) (Supporting Information, p S14). The values of $k_{-1,H}$ are 0.9 × 10^{-4} and 5 × 10^{-7} s^{-1} for Ru(η^6-C_6Me_6)(bpy)$(OC(H)O)^+$ and Ru(terpy)(bpy)$(OC(H)O)^+$, respectively.[38]

c. Reaction with CO. The rate constant for the reaction of CO with Ru(terpy)(bpy)H^+ was earlier reported[37] as 0.7 M^{-1} s^{-1}. The kinetics of CO addition to Ru(terpy)-(dmb)H^+ were followed by UV−vis (Supporting Information, p S15). The faster, CO-dependent phase yields a rate constant of 1.2(0.2) × 10^1 M^{-1} s^{-1} for eq 7a. A slower stage with k_{obs} = 1.3 × 10^{-3} s^{-1} is much faster than the aquation stage (eq 7b) found for the parent, unsubstituted bpy compound.[37]

$$Ru(terpy)(dmb)H^+ + CO + H_2O \rightarrow Ru(terpy)(dmb)(OCH_2(OH))^+ \quad (7a)$$

$$Ru(terpy)(dmb)(OCH_2(OH))^+ + H_3O^+ \rightarrow Ru(terpy)(dmb)(H_2O)^{2+} + CH_2(OH)_2 \quad (7b)$$

The reaction of CO with Ru(η^6-C_6Me_6)(bpy)$(H)^+$ was very slow, $k \leq 0.1$ M^{-1} s^{-1}; in some runs, the first few minutes gave oscillatory absorbance-time traces. Preliminary work was also carried out with the water-soluble derivative $Na_2Re(CO)_3$(dcb)H. The observations suggest

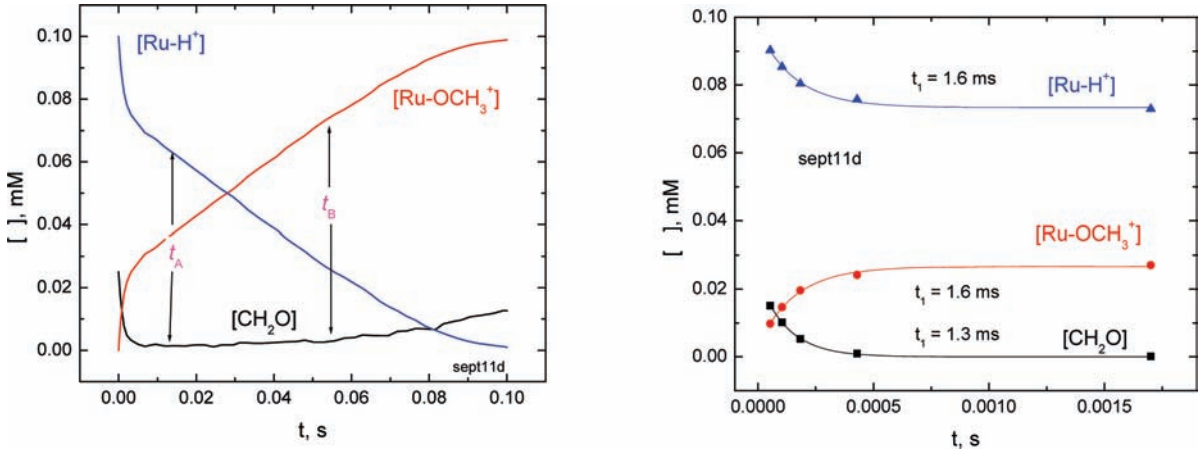

Figure 7. Left: Stochastic simulation[70] of the mechanism eq 8 and eq 10 with $k_{10} = 1 \times 10^7\ M^{-1}\ s^{-1}$, $k_8 = 0.022\ s^{-1}$, $k_{-8} = 50\ s^{-1}$, $[CH_2(OH)_2] = 0.05\ M$, $[CH_2O] = 2.50 \times 10^{-5}$ M, and $[RuH^+] = 0.1$ mM. Right: A blowup of the initial phase (points), $t = 0$ to $t = t_B$, and exponential fit (solid curve) to the points. The k_{obs} values for the consumption of RuH^+ and the formation of Ru-OCH_3^+, 625 s^{-1}, are roughly those expected for (excess) $[RuH^+] = 0.1$ mM and $k_{10} \sim 0.5 \times 10^7\ M^{-1}\ s^{-1}$.

a rate constant of $\sim 0.6\ M^{-1}\ s^{-1}$ for the reaction with CO in water.

d. Reaction with CH_2O. In water, formaldehyde is present as both hydrated and dehydrated forms (eq 8), with the hydrate being the dominant form.

$$CH_2(OH)_2 \rightleftarrows CH_2O + H_2O \quad K_{dehyd} = 4.4\times10^{-4}\ k_8, k_{-8} \qquad (8)$$

The rate constants for dehydration and hydration (k_8, k_{-8}), as used here, represent a composite rate constant for given conditions. In the pH 9.2 borate buffer, the values are approximately 0.022 s^{-1} and 50 s^{-1}.[68,69] In principle, the metal hydride may react with either or both forms of the aldehyde.

$$Ru\text{-}H^+ + CH_2(OH)_2 \rightarrow Ru(OCH_3)^+ + H_2O \quad k_9 \qquad (9)$$

$$Ru\text{-}H^+ + CH_2O \rightarrow Ru(OCH_3)^+ \quad k_{10} \qquad (10)$$

Reaction via eq 9 gives rise to simple second-order kinetics (pseudo-first-order in hydride in the case of a great excess of formaldehyde), with $-d[MH]/dt = k_{meas}[CH_2(OH)_2][MH]$ and $k_{meas} = k_9$. The behavior expected for reaction via eq 10 with the steady-state approximation for $[CH_2O]$, $-d[RuH^+]/dt = (k_8k_{10}[CH_2(OH)_2][RuH^+])/(k_{-8} + k_{10}[RuH^+])$, is less simple and determined by the competition between water and $Ru-H^+$ for the dehydrated form of formaldehyde. When $k_{-8} \gg k_{10}[RuH^+]$ and formaldehyde is in great excess, the kinetics are again pseudo-first-order in the hydride complex, but with $k_{meas} = K_{dehyd}k_8$. However, when $k_8[RuH^+] \gg k_{-8}$, the kinetics are zero-order in $[RuH^+]$. Furthermore, there is a chance that the approach to the steady state may be observed under some conditions. This is illustrated in Figure 7, a CKS[70] simulation of eqs 8 and 10, with the parameters and conditions given in the caption.

Between $t = 0$ and $t = t_A$ is a stage corresponding to the approach to the steady state. It is detectable under these conditions because the initial, equilibrium concentration of the dehydrate is comparable to (i.e., ~25% of) the initial concentration of the metal hydride. This stage is followed by one (from t_A to t_B) in which the rate of the $Ru-H^+$ reaction is independent of $[Ru-H^+]$. The $[CH_2O]$ is depressed from its equilibrium value during this stage.

MH = Ru(terpy)(bpy)H$^+$. Earlier, we reported[37] that the reaction of Ru(terpy)(bpy)H^+ with formaldehyde is rapid, with $k_{10} \sim 10^6\ M^{-1}\ s^{-1}$. Using the CKS simulation results, we here revise that estimate upward to $\sim 10^7\ M^{-1}\ s^{-1}$. What we did not appreciate earlier (Supporting Information for ref 37) was the presence of a zero-order stage in the hydride complex. Analyses of the data according to both first-order and zero-order rate laws are given in the Supporting Information. Results of both analyses are consistent with a value $k_{10} = (6 \pm 4) \times 10^6\ M^{-1}\ s^{-1}$.

MH = Ru(η^6-C_6Me_6)(bpy)(H)$^+$. Studied with 0.1 mM Ru(η^6-C_6Me_6)(bpy)H^+ in a 1 mM $Na_2B_4O_7$ buffer (pH 9.2), the reaction was first-order in the concentration of the hydride complex and first-order in formaldehyde (Figure 8) with a slope $k_{meas} = 0.50\ M^{-1}\ s^{-1}$; for the keto form, $K_{hyd} = 2.3 \times 10^3$, the rate constant k_{10} is then $1.1 \times 10^3\ M^{-1}\ s^{-1}$ at 25 °C.

Of course, the observed kinetics cannot rule out parallel reaction via both forms of formaldehyde (eqs 9, 10). To gain some insight into this issue, we studied the reaction of the hydride complex with methanol, a model for eq 9 (although the free-energy change is greater for the reduction of methanol than for the reduction of formaldehyde hydrate by >6 kcal/mol). Figure 9 compares the results, from which we conclude that $k_9 < 0.01\ M^{-1}\ s^{-1}$ and that reduction of formaldehyde occurs via reaction 10 with $k_{10} = 1 \times 10^3\ M^{-1}\ s^{-1}$ for Ru(η^6-C_6Me_6)(bpy)H^+.

3. Computational Results. Computational studies of Ru(II)terpyridyl compounds have been reported recently.[71−73] Table S4 (Supporting Information) summarizes

(68) Bell, R. P.; Evans, P. G. *Proc. R. Soc. London, Ser. A* **1966**, *291*, 297–323.
(69) Greenzaid, P.; Luz, Z.; Samuel, D. *Trans. Faraday Soc.* **1968**, *64*, 2780–2786.
(70) CKS, Chemical Kinetics Simulation. http://www.almaden.ibm.com/st/computational_science/ck/?cks (accessed Sep 2010).

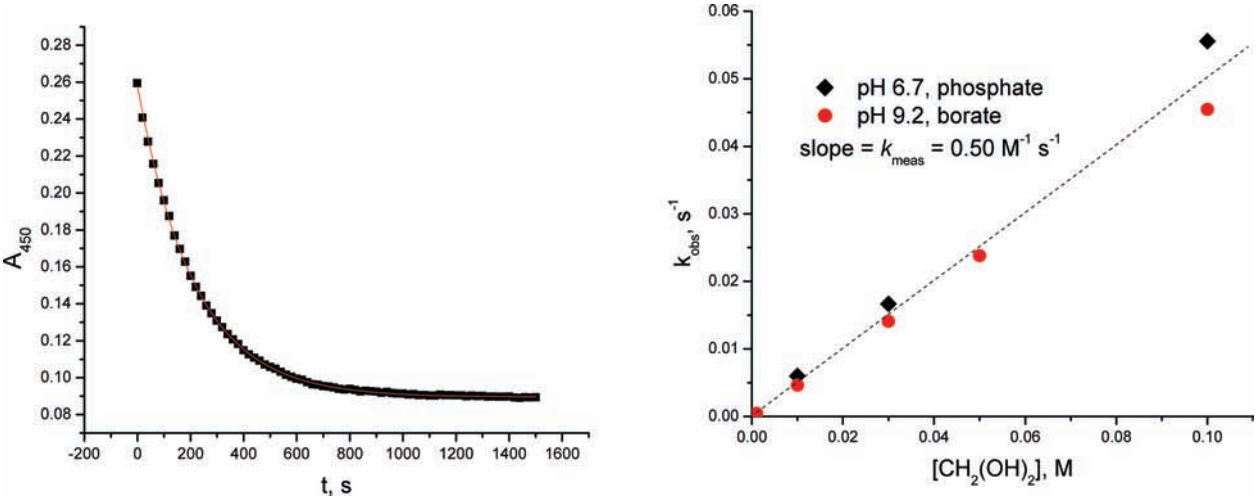

Figure 8. Kinetics observations for the reaction of Ru(η^6-C_6Me_6)(bpy)H^+ with formaldehyde at pH 6.7 and pH 9.2. Left: absorbance vs time (points) with fit to exponential (curve). Ru(η^6-C_6Me_6)(bpy)H(TFMS), 0.01 M $CH_2(OH)_2$, $Na_2B_4O_7$ 1 mM, 450 nm, t_1 = 214 s. Right: dependence of k_{obs} on formaldehyde concentration in pH 6.7 phosphate (black diamonds) and pH 9.2 borate (red circles) buffers.

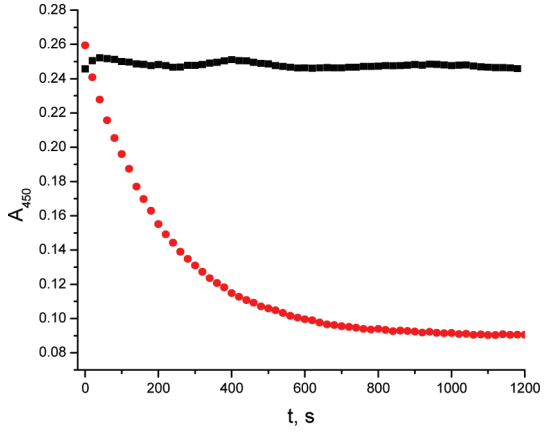

Figure 9. The 450-nm absorbance of 0.1 mM Ru(η^6-C_6Me_6)(bpy)H^+ in the presence of 0.01 M methanol (top trace) and 0.01 M formaldehyde at pH 9.2 with 1 mM $Na_2B_4O_7$.

structural parameters calculated for the reactants and products. In Table 2, experimental and calculated properties are listed for comparison. The Ru−H distance determined by X-ray diffraction is shorter than the calculated values. The measured M−H stretching frequencies are lower than the computed values. Interestingly, calculations for both hydride complexes predict lengthening of the Ru−N or Ru−C bond trans to hydride. This is verified in the structure reported for Ru(η^6-C_6Me_6)(bpy)$(H)^+$ (Ru−C2 is 0.1 Å longer than the other Ru−C distances[51]). In both experimental and computed structures, the formate C−O bonds differ in length. However, in the computed structures, the C−O distance for the O bonded to Ru is longer, while in the X-ray structures, that C−O bond is shorter. The parameter $z(H^-)$ is the calculated Mulliken charge on the hydride ligand. It is interesting to also

Table 2. Experimental and Calculated Structural Parameters

complex	property	exptl	calcd[a]
Ru(η^6-C_6Me_6)(bpy)$(H)^+$	d Ru−H, Å	1.51(4)[b]	1.61
	ν_{MH}, cm^{-1}	1908[b,c]	2064
Ru(terpy)(bpy)$(H)^+$	ν_{MH}, cm^{-1}	1827	1994
Ru(terpy)(bpy)$(HCO_2)^+$	d Ru to O, Å	2.09(1)[c]	2.06
	d (Ru)O to C, Å	1.22(3)[c]	1.32
	d O to C, Å	1.26(3)	1.21
	d H−C, Å	0.90(17)[c]	1.11
Ru(η^6-C_6Me_6)(bpy)$(HCO_2)^+$	d Ru to O, Å	2.107(2)[d]	2.076
	d (Ru)O to C, Å	1.250(3)[d]	1.32
	d O to C, Å	1.229(3)	1.22
	d H to C, Å	1.05(3)[d]	1.11

[a] For n = 0 water. [b] Ref 47. [c] Ref 51. [d] Ref 75.

compare the computed charges of hydride ligands. Bortoluzzi[74] found that with M = Fe the hydride charge is more negative (−0.23) than for M = Ru (−0.13) in complexes of the type M(bpy)$(PH_3)_3(H)^+$.

The electronic absorption spectra calculated for **1** and **2** are shown in Figure 10. The assignments and observed and calculated absorption maxima are listed in Table 3, and frontier orbitals are depicted in Figures S21 and S22 (Supporting Information). The measured and calculated electronic absorption spectra are in very good agreement.

4. Solvent Dependence of Rates and Spectra. The electronic spectra of the terpyridyl−bipyridyl hydride complexes **1** and **3** exhibit distinct maxima at > 500 nm and at ~385 nm in organic solvents (see Figure S2, Supporting Information). By contrast, the higher energy band is not well resolved in water. Spectral features as a function of the solvent are listed in Table S3 (Supporting Information). The correlations of both MLCT bands for the hydride complexes Ru(terpy(bpy)H^+ and Re(bpy)-$(CO)_3H$ (squares)[7,76] and the rate constants for insertion

(71) Borg, O. A.; Godinho, S. S. M. C.; Lundqvist, M. J.; Lunell, S.; Persson, P. *J. Phys. Chem A*. **2008**, *112*, 4470–4476.
(72) Jakubikova, E.; Chen, W.; Dattelbaum, D. M.; Rein, F. N.; Rocha, R. C.; Martin, R. L.; Batista, E. R. *Inorg. Chem*. **2009**, *48*, 10720–10725.
(73) Wang, L.-P.; Wu, Q.; Van Voorhis, T. *Inorg. Chem*. **2010**, *49*, 4543–4553.
(74) Bortoluzzi, M.; Bordignon, E.; Paolucci, G.; Pitteri, B. *Polyhedron* **2007**, *26*, 4936–4940.
(75) Ogo, S.; Abura, T.; Watanabe, Y. *Organometallics* **2002**, *21*, 2964–2969.
(76) Dietrich, J.; Schindler, S. *Z. Anorg. Allg. Chem*. **2008**, *634*, 2487–2494.

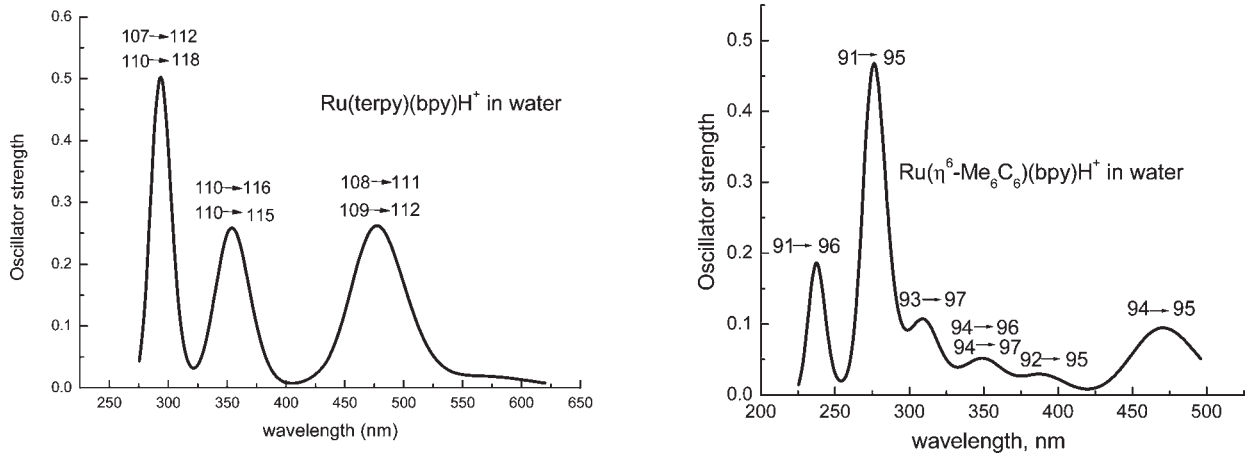

Figure 10. Calculated UV−vis spectra of Ru(terpy)(bpy)H^+ and Ru(η^6-C_6Me_6)(bpy)H^+ in water. The numbers identify the molecular orbitals involved in the transition.

Table 3. Assignments and Observed and Calculated Absorption Maxima (for Water Unless Otherwise Noted)

Ru(terpy)(bpy)H^+				Ru(η^6-C_6Me_6)(bpy)H^+		
	λ_{max}, nm			λ_{max}, nm		
origin	calc.	obs.	obs[a]	origin	calc.	obs.
MLCT (Ru to terpy + bpy)	575		650	MLCT (Ru + H to bpy)	460	450
MLCT (Ru to terpy + bpy)	477	486	530	MLCT (Ru + H to bpy + C_6Me_6)	390	410
				MLCT (Ru + H to bpy)	345	350
MLCT (Ru to terpy + bpy)	354	366	380	MLCT (Ru to bpy)	310	319 sh
π(terpy)−π^*(terpy + bpy)		315	310	bpy π−π^*	270	284
π(terpy)−π^*(terpy + bpy)	293	291		bpy π−π^*	230	241

[a] For solvent acetonitrile as given by Konno et al.[47]

of CO_2 are plotted in Figure 11. The greater slope for Re(bpy)$(CO)_3$H is likely due to solvent interactions with the three carbonyl ligands.

Discussion

1. Energetics of Hydride Transfer Pathways. The rate constants determined in this study, as well as some reported earlier, are summarized in Table 4. The first hydride ion acceptor listed is H_3O^+. Protonation of transition metal hydride complexes is now recognized as a potentially complex process.[77] The initial site of protonation can be the hydride, the metal, or a basic ligand. Often, an η^2-H_2 complex is an intermediate on the path to H_2 loss. Although this acceptor is included in Tables 4 and 8 (*vide infra*), the reactions of the metal hydride complexes with acid are believed to be different in character from the reactions with C_1 species.

Stoichiometric hydride ion transfer can proceed via any of the three pathways depicted in Scheme 2. For carbon centers, two pathways are in evidence: (1) hydride ion transfer (HIT) and (2) electron transfer (ET), followed by H atom transfer (HAT) (or electron transfer, followed by

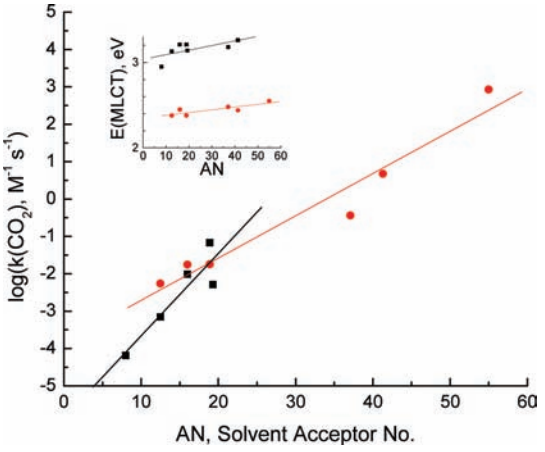

Figure 11. The logarithm of the CO_2 insertion rate constant vs solvent acceptor number. Inset: Energy of the MLCT band vs acceptor number. For both, Re(bpy)$(CO)_3$H (squares)[7,76] and Ru(terpy)(bpy)H^+ (circles).[37,47].

H^+ (PT) and electron transfer).[79−81] These are illustrated in Scheme 2, where DH refers to the hydride donor and A^+ to the hydride or electron acceptor and where hydrogen-atom transfers are horizontal, electron-transfer reactions are vertical, and hydride-ion transfer occurs on the diagonal. For metal hydrides, the low intrinsic barrier to H-atom transfer[82] leads to the additional consideration of

(77) Besora, M.; Lledós, A.; Maseras, F. *Chem. Soc. Rev.* **2009**, *38*, 957–966.
(78) Haasnoot, H. G.; Hinrichs, W.; Weir, O.; Vos, J. G. *Inorg. Chem.* **1986**, *25*, 4140–4143.
(79) Fukuzumi, S.; Koumitsu, S.; Hironaka, K.; Tanaka, T. *J. Am. Chem. Soc.* **1987**, *109*, 305–316.
(80) Cheng, J.-P.; Lu, Y.; Zhu, X.; Mu, L. *J. Org. Chem.* **1998**, *63*, 6108–6114.
(81) Yuasa, J.; Yamada, S.; Fukuzumi, S. *J. Am. Chem. Soc.* **2006**, *128*, 14938–14948.

Table 4. Rate Constants for Hydride Transfer to H^+ and C_1 Species in Water (This Study, unless Otherwise Noted)

	k, M^{-1} s^{-1}			
hydride complex	H_3O^+	CO_2	CO	H_2CO
$Ru(tpy)(bpy)H^+$	$\geq 2 \times 10^{4a}$	8.5×10^{2b}	0.7^b	$(6 \pm 4) \times 10^6$
$Ru(\eta^6\text{-}C_6Me_6)(bpy)(H)^+$	2.2×10^1	0.77	≤ 0.1 M^{-1} s^{-1}	1.1×10^3
$Ru(tpy)(dmb)H^+$			$1.2(0.2) \times 10^1$	
$Re(CO)_3(dcb)H^{2-}$		≥ 30	0.6	
$Ru(bpy)_2(CO)H^+$	1.1×10^{-1c}			

[a] Complex reaction; see text. [b] Ref 37. [c] Ref 78 at 303 K.

Scheme 2. Hydride Transfer Pathways

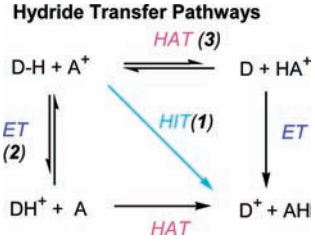

initial H-atom transfer, followed by electron transfer (top horizontal, pathway 3). (Note that the H-atom transfer may also be accomplished by different mechanistic pathways: initial proton, electron, or H-atom transfer; indeed, hydride transfer from NADH analogues to quinones,[79] nonheme oxoiron(IV),[83] and Mn(V) oxoporphyrin[84] complexes proceeds via an electron-transfer pathway.)

Scheme 3 shows the thermodynamic cycles used.

From studies of the equilibration of the Ru(II) hydride complexes with CO_2/formate, hydricity values of the hydride complexes can be evaluated. With the use of $\Delta G°_{H^-}$ (HCO_2^-) = +34.8 (+23) kcal/mol,[37] hydricities of +22 (+10.4) and +31 (+18.8) kcal/mol are derived for **1**(**H**) and **2**(**H**), respectively. Two estimates of the acidity of H_2, differing by 9 pK units, have been given: Here, values derived from the older (and very widely used) value 31[85] are used for H_2, but in some instances, values based on the more recent estimate of 22[86] are also given in parentheses.

We turn now to an analysis of the possible pathways shown in Scheme 2. To accomplish this, we need three sets of parameters for each reaction: the hydricities, the one-electron reduction potentials, and the bond-dissociation energies of the metal hydrides and the hydride acceptors that we have studied. These are derived in the Appendix and summarized in Tables 5−7.

Apart from CO (see below), hydride ion transfer (path 1, Scheme 2) is thermodynamically favorable as an elementary step for all of the acceptors listed in Table 8. Furthermore, initial electron transfer followed by H-atom transfer (path 2, Scheme 2) is excluded by the extremely small value of log(K_{ET}). That is, even assuming a rate constant of $k_{max} = 10^{10}$ M^{-1} s^{-1} for the subsequent H-atom transfer, the highest possible rate constant $K_{ET}k_{max}$ is many orders of magnitude smaller than the rate constant measured. The situation for CO and CH_2O and H-atom transfer (path 3, Scheme 2) is more complex. For both, log(K_{HAT}) is such that H-atom-initiated hydride ion transfer is probably viable. CO presents a special concern. Overall, hydride ion transfer to give HCO^- is extremely unfavorable; the overall reduction to formaldehyde must be driven by protonation of the carbon (and hydrolysis to yield the coordinated formaldehyde hydrate). For single-electron reduction of CO in water, hydration of the formyl radical ion is estimated as $> 10^4$ s^{-1}.[97]

2. Nature of the C=O Insertion Reaction. Rate constants for reactions of the Ru(II) hydride complexes with CO_2 are greater than for substitution on the corresponding aqua complexes, yet the primary product of the reaction is the O-bonded formate complex in both cases.[37,38] At least for $Ru(\eta^6\text{-}C_6Me_6)(bpy)(H)^+$, the M−H/M−D isotope is negligible. As shown in Figure 11, the reaction is extremely sensitive to solvent, with rates increasing with the Gütmann solvent acceptor number.[47] Detailed kinetics studies of reactions of analogous Rh(III) and Re(I) hydride complexes with CO_2 revealed very negative entropies and volumes of activation, taken to suggest an associative mechanism for the reactions.[76] The insertion of carbon dioxide into metal hydride bonds to yield formate complexes has been studied rather extensively on a theoretical level.[26,40−43,98−102] In all cases of which

(82) Song, J. S.; Bullock, R. M.; Creutz, C. *J. Am. Chem. Soc.* **1991**, *113*, 9862–9864.
(83) Fukuzumi, S.; Kotani, H.; Lee, Y.-M.; Nam, W. *J. Am. Chem. Soc.* **2008**, *130*, 15134–15142.
(84) Lee, J. Y.; Lee, Y.-M.; Kotani, H.; Nam, W.; Fukuzumi, S. *Chem. Commun.* **2009**, 704–706.
(85) Pearson, R. G. *J. Am. Chem. Soc.* **1986**, *108*, 6109–6114.
(86) Kelly, C. A.; Rosseinsky, D. R. *Phys. Chem. Chem. Phys.* **2001**, *3*, 2086–2090.
(87) Benderskii, V. A.; Benderskii, A. V. *Laser Electrochemistry of Intermediates*; CRC Press: Boca Raton, FL, 1995; p 253.
(88) Stanbury, D. M. *Adv. Inorg. Chem.* **1989**, *33*, 69–138.
(89) Schwarz, H. A.; Dodson, R. W. *J. Phys. Chem.* **1984**, *88*, 3643–3647.
(90) Kaim, W.; Reinhardt, R.; Sieger, M. *Inorg. Chem.* **1994**, *33*, 4453–4459.
(91) Rasmussen, S. C.; Ronco, S. E.; Mlsna, D. A.; Billadeau, M. A.; Pennington, W. T.; Kolis, J. W.; Petersen, J. D. *Inorg. Chem.* **1995**, *34*, 821–829.
(92) Pavlishchuk, V. V.; Addison, A. W. *Inorg. Chim. Acta* **2000**, *298*, 97–102.
(93) Shaw, A. P.; Norton, J. R.; Buccella, D.; Sites, L. A.; Kleinbach, S. S.; Jarem, D. A.; Bocage, K. M.; Nataro, C. *Organometallics* **2009**, *28*, 3804–3814.
(94) Wayner, D. D. M.; Parker, V. D. *Acc. Chem. Res.* **1993**, *26*, 287–294.
(95) Kim, E. H.; Bradforth, S. E.; Arnold, D. W.; Metz, R. B.; Neumark, D. M. *J. Chem. Phys.* **1995**, *103*, 7801.
(96) NIST Chemistry WebBook. http://webbook.nist.gov/chemistry/form-ser.html (accessed Sep 2010).
(97) Raef, Y.; Swallow, A. J. *J. Phys. Chem.* **1966**, *70*, 4072–4073.
(98) Hutschka, F.; Dedieu, A.; Eichberger, M.; Fornika, R.; Leitner, W. *J. Am. Chem. Soc.* **1997**, *119*, 4432–4443.
(99) Sakaki, S.; Ohkubo, K. *Inorg. Chem.* **1988**, *27*, 2020–2021.
(100) Sakaki, S.; Ohkubo, K. *Inorg. Chem.* **1989**, *28*, 2583–2590.
(101) Sakaki, S.; Musashi, Y. *J. Chem. Soc., Dalton Trans.* **1994**, 3047–3054.
(102) Musashi, Y.; Sakaki, S. *J. Am. Chem. Soc.* **2002**, *124*, 7588–7603.

Scheme 3. Thermodynamic Cycles for D−H and H_2

For D−H	$\Delta G°$	For H_2	$\Delta G°$
(3-1) Hydricity D−H ⇌ $D^+ + H^-$	$\Delta G°_{H^-}$ (D−H)	(3-5) H_2 Acidity H−H ⇌ $H^- + H^+$	$\Delta G°_{H^+}$ (H_2)
(3-2) Acidity D−H ⇌ $D^- + H^+$	$\Delta G°_{H^+}$ (D−H), pK_a	(3-6) NHE $2H^+ + 2e^-$ ⇌ H_2	$2E°$ (NHE)
(3-3) Homolysis D−H ⇌ D + H•	$\Delta G°_{H\cdot}$ (D−H)	(3-7) H_2/H• H_2 ⇌ 2H•	$\Delta G°_{H\cdot}$ (H_2)
(3-4) Reduction $D^+ + 2e^-$ ⇌ D^-	$2E°$ (D^+/D^-)	(3-8) H^+/H^- $H^+ + 2e^-$ ⇌ H^-	$2E°$ (H^+/H^-)

Table 5. Hydricities of Reactants/Products Examined in this Study in Water

reaction	$\Delta G°_{H^-}$, eV/molecule	$\Delta G°_{H^-}$, kcal/mol
H_2 ⇌ $H^+ + H^-$	+1.83	+42.1
H−CO_2^- ⇌ $CO_2 + H^-$	+1.48	+34
H−CO^- ⇌ $CO + H^-$	−0.76	−17.5
H−CH_2O^- ⇌ $CH_2O + H^-$	+1.57	+36
$RuLH^+ + H_2O$ ⇌ $RuL(H_2O)^{2+} + H^-$		
L = (tpy)(bpy)	0.96	+22
L = (η^6 - C_6Me_6) (bpy)	1.35	+31

Table 6. Reduction Potentials (H_2O, 25 °C vs NHE unless Otherwise Noted) for One-Electron Reduction of C_1 Species[87] and Other Reactants/Products Examined in This Study

	couple	$E°$, V
i	$H^+ + e^-$ ⇌ H•	−2.3[a,88]
ii	H• + e^- ⇌ H^-	−0.03
iii	$CO_2 + e^-$ ⇌ CO_2^-	−1.90[89]
iv	$CO + H^+ + e^-$ ⇌ HCO	−1.31
v	$H_2CO + e^-$ ⇌ CH_2O^-	−1.81[89]
viii	$Ru(terpy)(bpy)H^{2+/+}$	+0.5(3)[b]
ix	$Ru(\eta^6\text{-}C_6Me_6)(bpy)H^{2+/+}$	+1.3(2)[c,90]
x	$Ru(terpy)(bpy)(S)^{2+/+}$	−1.12[d,91]
xi	$Ru(\eta^6\text{-}C_6Me_6)(bpy)(S)^{2+/+}$	−0.60[e,90]

[a] pH 0. [b] Irreversible $Ru(terpy)(bpy)H^{2+/+}$ at −0.12 V vs $Ag/AgNO_3$ corresponds to +0.43 V vs NHE.[47,91,92] For $Ru(tpy)(bpy)(Cl)^{2+/+}$, the $Ru^{III/II}$ couple is at +0.49 V[47] vs $AgNO_3$/Ag and +1.04 V[92] vs NHE; the oxidation of the corresponding hydride complex is expected[93] to occur at a 0.4 to 0.6 V lower potential. Thus, +0.5(2) V vs NHE is estimated. [c] For $Ru(\eta^6\text{-}C_6Me_6)(bpy)(Cl)^{2+/+}$, the $Ru^{III/II}$ couple is at +1.25 V[90] vs $Fc^{+/0}$ and +1.80 V[92] vs NHE; the oxidation of the corresponding hydride complex is expected[93] to occur at a 0.4 to 0.6 V lower potential. Thus, +1.3(2) V vs NHE is estimated. [d] Versus SCE in CH_3CN. [e] For $Ru(\eta^6\text{-}C_6Me_6)(bpy)(S)^{2+/+}$, a two-electron process that presumably occurs near the 2+/1+ potential, for the acetonitrile complex at −1.23 V vs Fc+/0, which corresponds to −0.60 V vs NHE.

we are aware the transition state has a four-centered structure of the type depicted in Figure 12. In some cases, weak metal bonding to oxygen precedes transition-state formation; in others, not.

Generally speaking, the activation free energy decreases as the free-energy change becomes more negative, which, in turn, is favored by strongly electron donating ligands, polar solvents, and hydrogen-bonding solvents or substituents. Free-energy profiles and molecular structures obtained from our computational studies of the two hydride complexes are presented in Figure 13. Selected bond distances are given in Table S6 (Supporting Information).

As found for other systems[40−43] (but with organic solvents only), the reaction is an "insertion reaction". The transition state is very product-like with Ru−H elongated by 0.6 Å and C−H bond formation essentially complete, d(C−H) = 1.15 and 1.154 Å for $Ru(terpy)(bpy)H^+$ and $Ru(\eta^6\text{-}C_6Me_6)(bpy)H^+$, respectively, compared to 1.109 in the product, but Ru−O(formate) bond formation is not very advanced, 3 Å compared to 2.1 Å, with that bond

Table 7. Energetics of H Atom Transfer Reactions in Water,[a] kcal/mol

reaction	$\Delta_{f,g}°H$	$\Delta G°_{rxn}$
H• ⇌ $1/2H_2$	−48.6	−52.8[94]
CO_2 + H• ⇌ H−CO_2	+13.3[95]	+9.1
CO + H• ⇌ H−CO	−12.6	−16.8
CH_2O + H• ⇌ H−CH_2O	−20	−24.2
CH_2O + H• ⇌ CH_2OH	−26	−30
$RuLH^+ + H_2O$ ⇌ $RuL(H_2O)^+ + H^•$		
L = (terpy)(bpy)		21.8
L = (η^6-C_6Me_6)(bpy)		61

[a] We used the differences (product − reactants) between tabulated[96] heats of formation for the first five reaction entries. To obtain the solution phase values, we assume that the radical and neutral species have identical values and correct for the entropy and solvation of the hydrogen atom. H_g ⇌ H_s; S ⇌ H_2O, + 4.2 e.u.

Table 8. Rate Constants (k_{meas}) for Hydride-Ion Transfer from Ru(terpy)(bpy)H+ (**1**) and Ru(η^6-C_6Me_6)(bpy)$(H)^+$ (**2**) and Logarithms of Estimated Equilibrium Constants for Hydride Ion, Electron, and H-Atom Transfer

	k_{meas}, M^{-1} s^{-1}		log(K_{HIT})		log(K_{ET})		log(K_{HAT})	
reactant	**1**	**2**	**1**	**2**	**1**	**2**	**1**	**2**
H_3O^+	$\geq 2 \times 10^4$	2.2×10^1	14.8	8.2	−47	−61		
CO_2	8.5×10^2	0.7	8.8	2.2	−35	−54	−23	−58
CO	0.7	≤0.1	−29	−36	−31	−44	−3.7	−32
CH_2O	$(6 \pm 4) \times 10^6$	1.1×10^3	10.3	3.7	−39	−53	1.8	−26

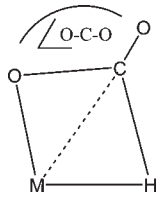

Figure 12. The four-centered transition state for insertion of CO_2 into an M−H bond is characterized by M−O, C−O, C−H. and M−H distances and the O−C−O angle.

formation requiring a rotation of the formate ion. Also noteworthy is the observation that for $Ru(terpy)(bpy)(H)^+$ the Ru−N(bpy) bond trans to hydride is lengthened in the ground state (2.19 Å vs 2.11 Å for the other pyridyl group) but shortened in the transition state (2.03 Å vs 2.12 Å). Thus, the hydride ion transfer is strongly coupled to the motion of the trans nitrogen.

An abbreviated reaction scheme drawn approximately to scale is shown in Scheme 4. It is the RuH stretching mode and the CO_2 ν_{2a} stretch that take the reactants to the transition state.

In the subsequent step, the transition state is converted to product by relaxation of the formate ion and formation of the Ru−O bond. It is common to consider the nature of transition states as early (more like reactants) or late (more like products). In terms of the concept of x, the reaction coordinate, which varies between 0 and 1 as reactants proceed to products, $x < 0.5$ corresponds to an

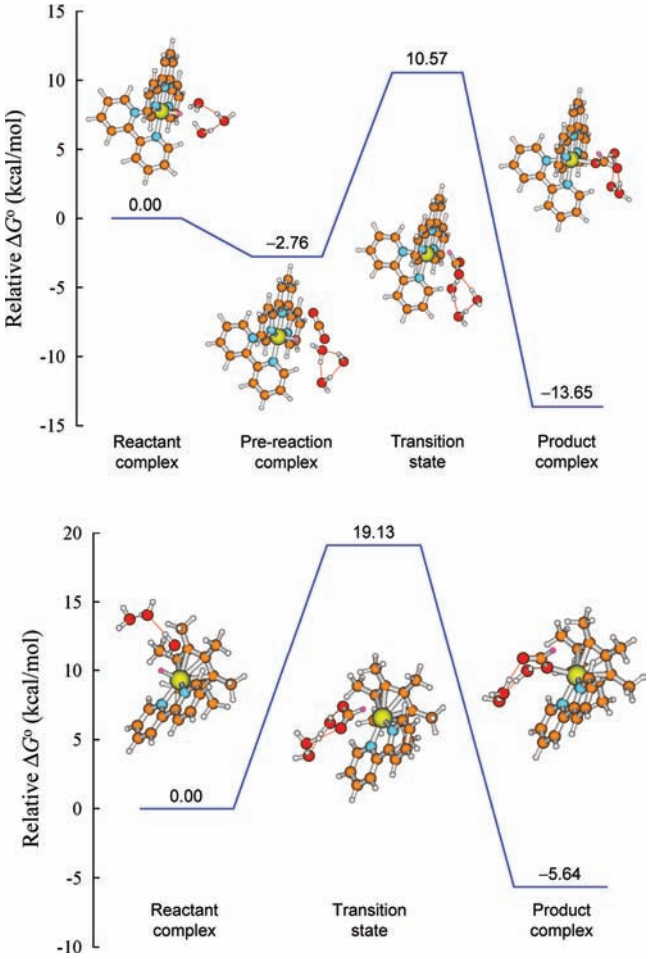

Figure 13. Free-energy profiles (ΔG_v[42] and structures obtained for the reaction of (top) Ru(terpy)(bpy)H^+ and (bottom) Ru(η^6-C_6Me_6)(bpy)-$(H)^+$ with CO_2 in the presence of three water molecules.

Scheme 4. CO_2 Insertion

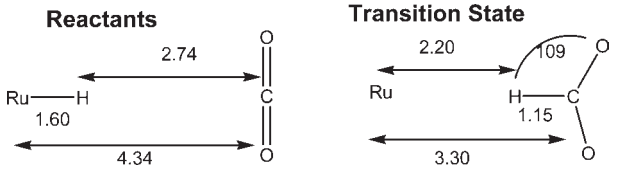

early transition state, and $x \gg 0.5$ corresponds to a late one. Estimating the position of the transition state through the free-energy relationship eq 11[103,104]

$$x^{\ddagger} = \Delta G^{\ddagger}/(2\Delta G^{\ddagger} - \Delta G^{\circ}) \qquad (11)$$

yields $x^{\ddagger} = 0.33$ and 0.47 for CO_2 insertion into Ru(terpy)-(bpy)$(H)^+$ and Ru(η^6-C_6Me_6)(bpy)$(H)^+$, respectively

Scheme 5. Decarboxylation of Formate Complex

The reverse of the insertion step determines the rate of CO_2 loss from the formate complex and is also of interest.[105−109] The decarboxylation step (Scheme 5) exhibits a small, normal isotope effect $k_H/k_D = 1.15(0.1)$ for Ru(η^6-C_6Me_6)(bpy)$(OC(H)O)^+$ and rate constants of $0.9 \times 10^{-4}\ s^{-1}$ and $5 \times 10^{-7}\ s^{-1}$ for Ru(η^6-C_6Me_6)(bpy)(OC-$(H)O)^+$ and Ru(terpy)(bpy)$(OC(H)O)^+$, respectively.[38] For the decarboxylation of (η^5-C_5H_5(NO)(PPh_3)Re(OC-$(H)O)^+$, $k_H/k_D = 1.55$,[110] consistent with sizable C−H bonding in the transition state.[106]

The Role of Solvent/Water. The high sensitivity of the rate of hydride transfer to solvent has already been noted with rate constants increasing with solvent acceptor number.[37,47] The role of water solvent is receiving attention in the computational community.[111] One motivation for our computational study was to try to understand the origin of the high sensitivity of the insertion process to solvent, particularly water. Table S6 (Supporting Information) provides a detailed picture of the evolution of the transition state with an increasing number of waters.

The activation and net free-energy changes are in rather remarkable agreement with the experiment (Table S5, Supporting Information): for Ru(terpy)(bpy)H^+ with three H_2O's, the calculated reaction barrier ($\Delta G_v^{\dagger}$) and driving force (ΔG_v^{0}) are 10.6 and −13.7 kcal/mol, respectively, compared to the experimental values 13.5 and −12.2 kcal/mol. For Ru(η^6-C_6Me_6)(bpy)$(H)^+$ with three H_2O's, the calculated reaction barrier and driving force are 19.1 and −5.6, respectively, vs the experimental values 17.8 and −3.9 kcal/mol. Ohnishi et al.[42] compared the CO_2 insertion processes for Rh(III) and Ru(II) hydride complexes and concluded that the latter is a more facile process because of the greater strength of the Ru(II)−O(formate) bond. The results for the present system also exhibit this feature: the more exoergic reaction is the faster one.

Even in the absence of water, the transition state is very late, with the Ru−H bond greatly lengthened and the C−H bond significantly formed. The O−C−O angle is ca. 133°. As water is added, the O atoms bound to carbon in CO_2 form hydrogen bonds with the water, the O−C−O angle increases slightly, and the Ru−H distance lengthens even more, as do Ru−C and Ru−O. The C−H bond shortens. As the water content increases, the transition state occurs later and later on the reaction coordinate, and the imaginary frequency, ν_i, drops in absolute value, indicating that the curvature of the surface at the transition state decreases with increasing water content.

Examination of our results yields no crisp conclusion about the role of water. Energetics for the two Ru(II)

(103) Wigfield, D. C. *Tetrahedron* **1979**, *35*, 449–462.
(104) Kresge, A. J. *Can. J. Chem.* **1974**, *52*, 1897–1903.
(105) Darensbourg, D. J.; Longridge, E. M.; Holtcamp, M. W.; Klausmeyer, K. K.; Reibenspies, J. H. *J. Am. Chem. Soc.* **1993**, *115*, 8839–8840.
(106) Darensbourg, D. J.; Wiegreffe, P.; Riordan, C. G. *J. Am. Chem. Soc.* **1990**, *112*, 5759–5762.
(107) Sullivan, B. P.; Bruce, M. R. M.; O'Toole, T. R.; Bolinger, C. M.; Megehee, E.; Thorp, H.; Meyer, T. J. Electrocatalytic Carbon Dioxide Reduction. In *Catalytic Activation of Carbon Dioxide*; American Chemical Society: Washington, DC, 1988; pp 52−90.
(108) Darensbourg, D. J.; Bauch Christopher, G.; Ovalles, C. Metal-Induced Transformations of Carbon Dioxide. In *Catalytic Activation of Carbon Dioxide*; American Chemical Society: Washington, DC, 1988; pp 26−41.
(109) Fukuzumi, S.; Kobayashi, T.; Suenobu, T. *J. Am. Chem. Soc.* **2010**, *132*, 1496−1497.
(110) Merrifield, J. H.; Gladysz, J. A. *Organometallics* **1983**, *2*, 782–784.
(111) Garand, E.; Wende, T.; Goebbert, D. J.; Bergmann, R.; Meijer, G.; Neumark, D. M.; Asmis, K. R. *J. Am. Chem. Soc.* **2009**, *132*, 849–856.

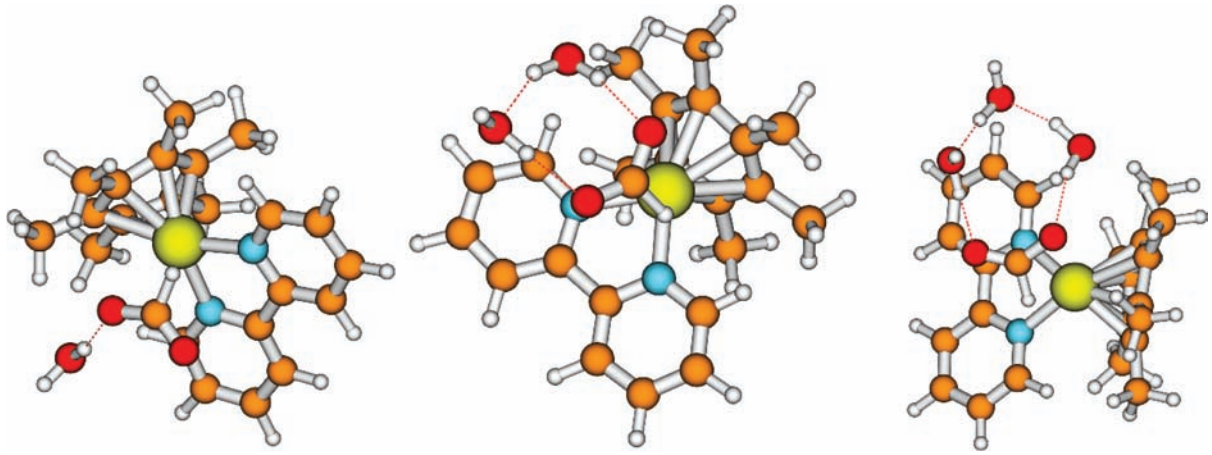

Figure 14. Transition state structures for Ru(η^6-C_6Me_6)(bpy)H^+ with one, two, and three water molecules.

hydride complexes studied were summarized in Table S5 (Supporting Information). In accord with the experiment, the barrier is smaller for Ru(terpy)(bpy)H^+ in water. For both hydride complexes, activation enthalpies drop 5−6 kcal per added water molecule, but the free energies of activation vary much less. The interactions of reactants, transition states, and products with water are strongly influenced by hydrogen bonding of water to the formate ion and to itself, as illustrated in Figure 14 for the transition-state structures for Ru(η^6-C_6Me_6)(bpy)H^+ with one, two, and three water molecules.

In the reactant and precomplex stage, a water H is always oriented toward the hydride ligand, consistent with the latter serving as a hydrogen-bond acceptor, with $d(H^- \cdots H{-}OH)$ = 1.7−1.9 Å, comparable to distances inferred for Cp*Fe(dhpe)H (dhpe = 1,2-diphosphinoethane).[112] This distance lengthens with the successive addition of water molecules. In both transition states and products, water is strongly H-bonded to the oxygen atoms of formate.

In general, the solute−solvent dipole−dipole interactions experienced by reactants, transition states, and products are incorporated into the computational reaction model by application of the polarized continuum model (PCM) corrections. Hydride transfers as a function of the solvent have been studied at the PCM-B3LYP/BSII level for solvents ranging from heptane to water.[113] The energies of reactants, products, and transition states were found to drop with increasing dielectric constant. However, the transition states dropped more gradually so that the reaction barrier actually increased with increasing dielectric constant. Here, the PCM corrections for both transition states and products were found to decrease as the number of water molecules included increased (see Table S7, Supporting Information), with the magnitude of the correction being 7−9 kcal/mol greater for the transition state than for the product.

Concluding Remarks

Experimental and computational studies have shown that the reactions of two Ru(II) hydride complexes with CO_2 in water are best described as insertion: formation of the C−H bond of formate precedes formation of the Ru−O bond in the product formate complex. In terms of the bulk properties of solvent water, the acceleration of the insertion process in water is traceable to the thermodynamics of hydride ion formation.[37] The present computational studies indicate an important role for hydrogen-bonding in water. While we assume that the CH_2O reactions are similar to those of CO_2, computational work on formaldehyde insertion would be very worthwhile. Characterization of the mechanism of H_2 formation from the protonation of RuH^+ in water is incomplete; η^2-H_2 intermediates are likely but are yet to be well characterized experimentally or computationally. Most puzzling (and probably ultimately, most complex) is the reaction of Ru(terpy)(bpy)H^+ and Ru(terpy)(dmb)H^+ with CO, for which one-step hydride ion transfer is prohibitively endergonic because of the very low H^- affinity of CO.

Acknowledgment. This research was carried out at Brookhaven National Laboratory under contract DE-AC02-98CH10884 with the U.S. Department of Energy and supported by its Division of Chemical Sciences, Geosciences and Biosciences of the Office of Basic Energy Sciences. We thank M. Doherty for making some of the NMR measurements.

Appendix

I. Hydricities of C_1 Species. The hydricities of HCO_2^-, HCO^-, and H_3CO^- in water are estimated as +1.48, −0.76, and +1.57 eV (+34, −17.5, +36 kcal/mol), respectively, from the following considerations.

To obtain the values given in Table 1, we used the cycle:

$$CO_2 + 2H^+ + 2e^- \rightleftharpoons HCO_2H \quad +2E^0(CO_2/HCO_2H)$$

$$-[2H^+ + 2e^- \rightleftharpoons H_2 \quad 2E^0(H^+/H_2) = 0]$$

$$H^+ + H^- \rightleftharpoons H_2 \quad 0.059(pK_a(H_2)$$

$$\textbf{Net}: CO_2 + H^+ + H^- \rightleftharpoons HCO_2H$$

a. Hydricity of Formate Ion: $CO_2 + H^- = HCO_2^-$. We use the cycle in eqs A1−A5 in Scheme A1 to calculate the hydricity of the formate anion, $\Delta G°_{H^-}(HCO_2^-)$.

(112) Belkova, N. V.; Shubina, E. S.; Epstein, L. M. *Acc. Chem. Res.* **2005**, *38*, 624–631.
(113) Matsubara, T.; Hirao, K. *Organometallics* **2001**, *20*, 5056–5066.
(114) Latimer, W. M. *Oxidation Potentials*, 2nd ed.; Prentice-Hall: Englewood Cliffs, NJ, 1952.

Scheme A1[a]

$$H^+_{aq} + H^-_{aq} \rightleftharpoons H_{2(aq)} \quad \log(K) = 31.5 \tag{A1}$$

$$H_{2(g)} + CO_{2(g)} \rightleftharpoons HCO_2H_2 \quad \Delta G^\circ = +9.2 \text{ kcal/mol}; \quad \log(K) = -6.78 \tag{A2}$$

$$CO_{2(aq)} \rightleftharpoons CO_{2(g)} \quad \log(K) = 1.53 \text{ (from the solubility of } CO_2, 0.03 \text{ M)} \tag{A3}$$

$$H_{2(aq)} \rightleftharpoons H_{2(g)} \quad \log(K) = 3.097 \text{ (from the solubility of } H_2, 0.0008 \text{ M)} \tag{A4}$$

$$HCO_2H_{(aq)} \rightleftharpoons HCO^-_{2(aq)} + H^+_{(aq)} \quad \log(K) = -3.8 \text{ (from the ionization constant for formic acid)} \tag{A5}$$

$$\text{Net}: \; H^-_{aq} + CO_{2(aq)} \rightleftharpoons HCO^-_{2(aq)} \quad \log(K) = 25.05; \; -\Delta G^\circ_{H^-}(HCO^-_2) = +34 \text{ kcal/mol}, \; 1.48 \text{ eV} \tag{A6}$$

[a] **log(*K*) value in eq A1 from ref** 85**; Δ*G*° value in eq A2 from ref** 114**.**

Table A1. Estimation of the pK_a for H_2CO

model	$\Delta G°(X^-)_{aq}$	+ PA	− 267	$-\Delta G^0(HX)_{aq}$	= 1.36pK_a	pK_a
H_2C_2/HC_2^-	−71	392	−267	−3	51	37.5
HCN/CN^-	−75	392	−267	1.2	51.2	37.6

Table A2. Calculation of the Hydricity of HCO^-

reaction	property	Δ*G*°, eV/molecule
$H_2CO \rightleftharpoons H^+ + HCO^-$	pK^a = 37.5[a]	2.21
$CO + 2H^+ + 2e^- \rightleftharpoons H^2C(OH)_2$	E° = −0.09 V[b]	0.18
$H_2C(OH)_2 \rightleftharpoons H_2CO + H_2O$	$K = 1/2500$[69]	0.20
$H_2 \rightleftharpoons 2H^+ + 2e^-$	0	
$H^+ + H^- \rightleftharpoons H_2$	log $K = 31$[85]	−1.83
sum: $H^- + CO \rightleftharpoons HCO^-$	$-\Delta G°_{H^-}(HCO^-)$	0.76

[a] See Table 1A. [b] (pH 0).

Table A3. Calculation of the Hydricity of H_3CO^-

reaction	property	Δ*G*°, eV/molecule
$H_2C(OH)_2 + 2H^+ + 2e^- \rightleftharpoons CH_3OH$	E° (pH 0) = +0.24	−0.48
$H_2CO + H_2O \rightleftharpoons H_2C(OH)_2$	$K = 2500$[69]	−0.20
$CH_3OH \rightleftharpoons CH_3O^- + H^+$	pK_a = 16	0.94
$H_2 \rightleftharpoons 2H^+ + 2e^-$	0	0
$H^+ + H^- \rightleftharpoons H_2$	log $K = 31$[85]	−1.83
sum: $H_2CO + H^- \rightleftharpoons CH_3O^-$	$-\Delta G°_{H^-}(H_3CO^-)$	−1.57

b. Hydricity of Formaldehyde: CO + H⁻ = HCO⁻. The formyl anion is known in the gas phase,[115] $\Delta_f°H_g$ = 1.28 kcal/mol,[116] $\Delta_f°H_g$(HCO) = 10.0 kcal/mol.[117] We first need to estimate the pK_a of H_2CO in water, which has not been reported. This is obtained from the gas phase proton affinity (PA) of HCO^- = −392 ± 2 kcal/mol[118] and the relation[85] $-\Delta G^0(X^-)_{aq}$ = PA − 267 − ΔG^0-$(HX)_{aq}$ − 1.36pK_a. The two acid/conjugate base pairs that most closely resemble the H_2CO/HCO^- pair are H_2C_2/HC_2^- and HCN/CN^-. These are used as models for $\Delta G°(HX)_{aq}$ and $\Delta G°(X^-)_{aq}$ and, as shown in the table below, give identical estimates for pK_a (H_2CO). We then use the combination of equilibrium data shown in Table A1 to obtain the free-energy change for the reaction, $H^- + CO = HCO^-$. The hydricity then obtained for HCO^- is −0.76 eV or −17.5 kcal/mol. Table A2 gives the calculation of the hydricity of HCO^-.

c. Hydricity of Methoxide: CH₂O + H⁻ = CH₃O. Table A3 gives the calculation of the hydricity of H_3CO^-.

Supporting Information Available: Characterization of materials, kinetic studeis, experiments with Ru(terpy)(dmb)H^+, experiments with $Na_2Re(CO)_3$(dcb)H, solvent-dependent spectra, and selected computational results. This material is available free of charge via the Internet at http://pubs.acs.org.

(115) Nguyen, M. T. *Chem. Phys. Let*. **1988**, *145*, 200–204.
(116) da Silva, G.; Bozzelli, J. W.; Sebbar, N.; Bockhorn, H. *ChemPhysChem* **2006**, *7*, 1119–1126.
(117) da Silva, G.; Bozzelli, J. W. *J. Phys. Chem. A* **2006**, *110*, 13058–13067.
(118) Murray, K. K.; Miller, T. M.; Leopold, D. G.; Lineberger, W. C. *J. Chem. Phys*. **1986**, *84*, 2520–2525.